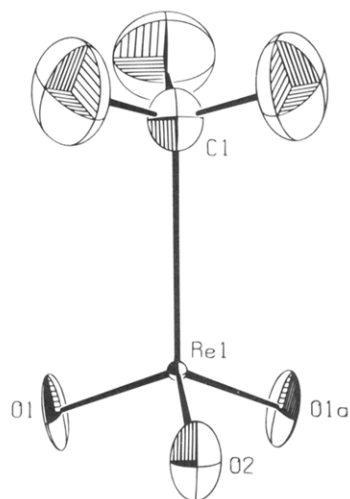


**Figure 1.** Typical transformations of “polymeric” methyltrioxorhenium (**1**). <sup>a</sup>Moist atmosphere, solid-state reaction.



**Figure 2.** Molecular structure of monomeric  $\text{CD}_3\text{ReO}_3$  at 5 K based on a powder neutron diffraction study (PLATON<sup>[7f]</sup> drawing showing the 90% probability ellipsoids). Important distances and angles of the *solid-state* structure are given in comparison (in brackets) with the *gas-phase* electron diffraction data:<sup>6</sup>  $\text{Re}=\text{O}1$ , 170.2(1);  $\text{Re}=\text{O}2$ , 170.2(2) [ $\text{Re}=\text{O}$  170.9(3)];  $\text{Re}-\text{C}$ , 206.3(2) [206.0(9)];  $\text{C}-\text{D}1$ , 108.2(3);  $\text{C}-\text{D}2$ , 109.6(2) [ $\text{C}-\text{H}$ , 110.5(1.2)];  $\text{C}-\text{Re}-\text{O}1$ , 105.9(1);  $\text{C}-\text{Re}-\text{O}2$ , 105.4(1) [ $\text{C}-\text{Re}-\text{O}$ , 106.0(2)];  $\text{O}1-\text{Re}-\text{O}2$ , 112.8(1);  $\text{O}1-\text{Re}-\text{O}1'$ , 113.2(1) [ $\text{O}-\text{Re}-\text{O}$ , 113.0(3)];  $\text{Re}-\text{C}-\text{D}1$ , 108.3(1);  $\text{Re}-\text{C}-\text{D}2$ , 108.1(1) [ $\text{Re}-\text{C}-\text{H}$ , 112(3)];  $\text{D}1-\text{C}-\text{D}2$ , 111.1(1);  $\text{D}2-\text{C}-\text{D}2'$ , 109.9(2). All distances are in pm and angles in deg.

cally) is slightly higher than the crystallographic density of monomeric MTO ( $\rho = 4.21 \text{ g cm}^{-3}$ , 23 °C), which consists of separated close-packed molecules in the solid state (Figures 2 and 3, neutron powder diffraction). Such a molecular arrangement obviously has no significant influence on the molecular structure of MTO—the molecular gas-phase<sup>6</sup> and solid-state structures are identical within methodological deviations (electron vs neutron diffraction; see data of Figure 2). The rhenium atom is located in the center of a nearly ideal tetrahedron formed by the methyl group and the three oxo ligands. The  $\text{Re}-\text{C}$  distance of 206.3(2) pm is slightly shorter than the corresponding distances observed for N-donor adducts of MTO and related alkyltrioxorhenium(VII) species ( $\text{RReO}_3$ ; quinuclidine ( $\text{R} = \text{alkyl}$ ), 207(1)–210.5(4) pm; *trans*- $\text{CH}_3\text{ReO}_3$ ; aniline, 209.5(5) pm;  $\text{CH}_3\text{ReO}_3$ ; toluidine, 210(1) pm;  $\text{CH}_3\text{ReO}_3$ ; *tert*-butylpyridine), 208.5(6) pm).<sup>7a–d</sup> Also the  $\text{Re}-\text{C}$  bond distance of the highly Lewis acidic peroxo species  $\text{CH}_3\text{Re}(\text{O}_2)_2\text{O}$  (204(1) pm, gas-phase electron diffraction)<sup>7e</sup> falls in the same range. The methyl group nearly satisfies  $\text{C}_{3v}$  symmetry and is arranged staggered with respect to the  $\text{ReO}_3$  fragment. No significant distortions of the methyl groups away from perfect tetrahedra could be observed. This study again demonstrates that there are no  $\alpha$ -agostic interactions between the metal center (formally  $\text{Re}^{\text{VII}}$ ,  $d^0$ ) and any of the hydrogen atoms.

The nearly identical densities of **1** and MTO suggest close packing for the structure model of polymer **1**, too. In contrast to the monomeric MTO, the polymeric form is insoluble in common organic solvents, in water, and in nonoxidizing mineral

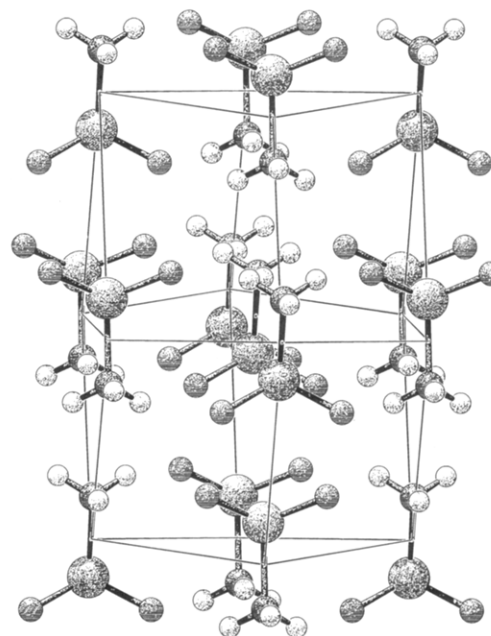
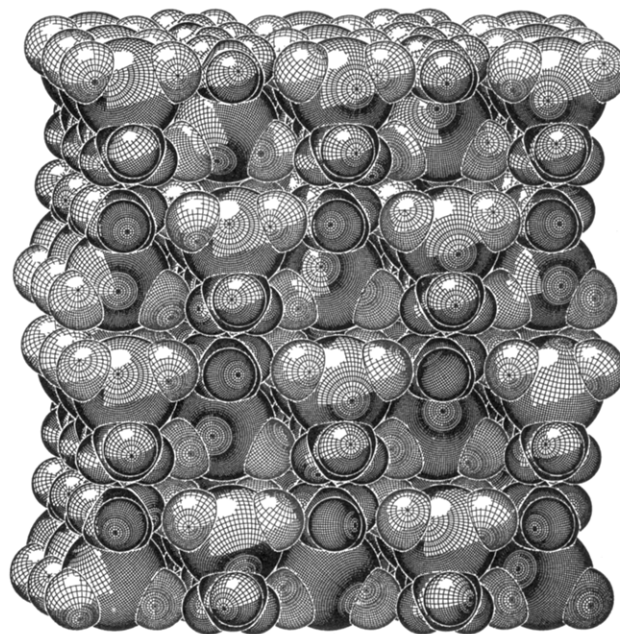


**Figure 3.** SCHAKAL<sup>[7g]</sup> drawings of the MTO structure (neutron diffraction). (top) Closed-packed  $\text{CH}_3\text{ReO}_3$  tetrahedra in the solid state. (bottom) MTO molecules located in the middle of a coordination polyhedron formed by 14 neighboring molecules.

acids. However, it readily reacts with dilute sodium hydroxide to yield perrhenate and methane. The solubility of **1** in aqueous hydrogen peroxide results from chemical “depolymerization” by formation of the peroxo complex  $\text{CH}_3\text{Re}(\text{O}_2)_2\text{O}\cdot\text{H}_2\text{O}$ <sup>8</sup> (Figure 1). The close chemical relationship between monomer and polymer is reflected by the unprecedented physical “depolymer-

(6) Herrmann, W. A.; Kiprof, P.; Rypdal, K.; Tremmel, J.; Blom, R.; Alberto, R.; Behm, J.; Albach, R. W.; Bock, H.; Soluki, B.; Mink, J.; Lichtenberger, D.; Gruhn, N. E. *J. Am. Chem. Soc.* **1991**, *113*, 6527–6537.

(7) (a) Herrmann, W. A.; Kühn, F. E.; Romão, C. C.; Huy, H. T.; Wang, M.; Fischer, R. W.; Kiprof, P.; Scherer, W. *Chem. Ber.* **1993**, *126*, 45–50. (b) Herrmann, W. A.; Herdtweck, E.; Weichselbaumer, G. *J. Organomet. Chem.* **1989**, *372*, 371. (c) Kiprof, P. Ph.D. Thesis, Technische Universität München, 1992. (d) Roesky, P.; Scherer, W. Unpublished. (e) Haaland, A.; Scherer, W.; Verne, H. P.; Volden, H. V.; Gundersen, S. Unpublished. (f) Spek, A. L. *PLATON-92–PLUTON-92, An Integrated Tool for the Analysis of the Results of a Single Crystal Structure Determination*; Acta Crystallogr., Sect. A **1990**, *46*, C34. (g) Keller, E. *SCHAKAL, A program for the Graphical Representation of Molecular and Crystallographic Models*; Kristallographisches Institut, Universität Freiburg, Germany, 1986/1988.

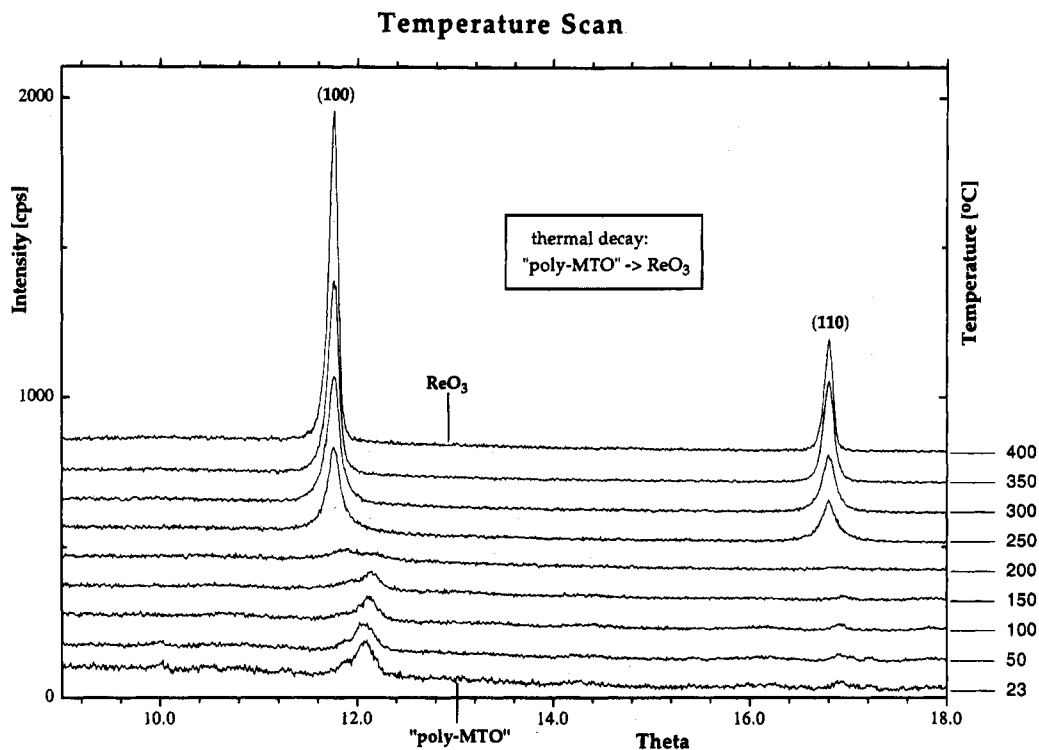


**Figure 4.** Thermal decomposition of “poly-MTO” (**1**). X-ray powder diffraction temperature scans at different temperatures [°C, right] and intensities [cps, left] (subsequent diffraction patterns are shifted by 100 cps). For further details, see the Experimental Section.

erization” of **1** under pressure: single crystals of monomeric MTO (plus some  $\text{ReO}_3$ ) are thus formed<sup>9</sup> (Figure 1).

Due to its striking lubricity, **1** can be spread on glass or paper, reminiscent of the well-known lubricants graphite and  $\text{MoS}_2$ . This property is indicative of a layer structure lacking strong interactions between adjacent layers. **1** appears as a flaky material in the SEM micrographs, once again typical of layer-structured compounds.

#### A “Two-Dimensional” Layer Model for Polymeric Methyltrioxorhenium

Thermal decomposition of moist samples of **1**, yielding  $\text{CH}_4$  and pure  $\text{ReO}_3$ , has been studied by X-ray powder temperature scans (Figure 4) and by thermogravimetry/mass spectrometry (TGA–MS, see Experimental Section).<sup>9</sup> The reaction enthalpy of this process ( $\Delta H = -8 \text{ kJ}\cdot\text{mol}^{-1}$ ) was determined calorimetrically (DSC experiment, see Experimental Section). Exhaustive demethylation occurs only in the presence of water, which provides the hydrogen equivalents:  $\{\text{H}_{0.5}[(\text{CH}_3)_{0.92}\text{ReO}_3]\}_\infty$  lacks approximately 0.4 equiv of acidic hydrogen for quantitative formation of methane. In contrast,  $\text{ReO}_2$  is produced when samples of **1** which are dried under high-vacuum conditions are heated above 250 °C on a Guinier camera (Figure 1).

$\text{ReO}_3$  and  $\{\text{H}_{0.5}[(\text{CH}_3)_{0.92}\text{ReO}_3]\}_\infty$  exhibit similar X-ray diffraction patterns: all  $hk0$  reflections of the  $\text{ReO}_3$  diffraction pattern have corresponding reflections with slightly shifted  $\theta$  values in the diffractogram of **1**. When these  $hk0$  reflections of “poly-MTO” are indexed, a hypothetical two-dimensional square unit cell with a lattice parameter of  $a = 3.728(1) \text{ \AA}$  results. The three-dimensional, cubic  $\text{ReO}_3$  has a lattice parameter of  $a = 3.748(1) \text{ \AA}$ .<sup>9,10</sup> At this stage it is important to stress that our two-dimensional model is not realistic and only hypothetical. It will therefore be expanded in the third dimension in the following sections (see The Three-Dimensional Model—A Double-Layer Structure with Intercalated Water).

(8) Herrmann, W. A.; Fischer, R. W.; Scherer, W.; Rauch, M. *Angew. Chem.* **1993**, *105*, 1209–1212; *Angew. Chem., Int. Ed. Engl.* **1993**, *32*, 1157–1160.

The two-dimensional relationship of **1** and  $\text{ReO}_3$  is best demonstrated by means of single-crystal electron diffraction. Thin crystal areas of “poly-MTO” showing typical diffraction patterns like the one of Figure 5a are oriented approximately parallel to the supporting foil. The pattern also corresponds to the square lattice constant obtained from X-ray powder diffraction ( $a = 3.73$  vs  $3.728(1) \text{ \AA}$ ). The symmetry of the recorded reciprocal  $hk0$  plane is in accord with the “two-dimensional” square space group  $p4mm$  (no. 11). Diffraction patterns slightly different from that of Figure 5a can also be recorded for different crystals of the same sample. Figure 5b shows a diffraction pattern with diffuse streaks along the  $[100]$  and  $[010]$  directions of the reciprocal lattice, which point to a disorder problem resulting from methyl deficiency. This phenomenon is discussed below.

On the basis of the above observations, we assume a  $\{\text{ReO}_2\}_\infty$ -layer structure element with a square motif expanded in two dimensions as a basic structure model. The rhenium atoms adopt the corner positions, while the oxygen atoms are located midway on the edges of the square unit cell. Both structures of  $\text{ReO}_3$  and **1** are essentially isotypic in two dimensions. The key data are compared with one another in Table 1.

#### Development of the “Two-Dimensional” Structure Model by Analytical Techniques and Chemical Studies

The layer structure evident from diffraction studies is based on a  $\{\text{ReO}_2\}_\infty$  network (Figure 6). How does this model fit the analytically determined net formula  $\{\text{H}_{0.5}[(\text{CH}_3)_{0.92}\text{ReO}_3]\}_\infty$ ? From simple stoichiometric considerations, one should expect approximately one methyl group, one oxo group, and about one-half extra hydrogen equivalent per rhenium atom in addition to  $\text{ReO}_2$ . Quantitative  $^1\text{H}$  NMR experiments indicate that every methyl group present ( $\text{CH}_3/\text{Re} = 0.92/1.0$ ) is bound to rhenium.<sup>1</sup> In addition, complete formation of  $\text{CH}_3\text{Re}(\text{O}_2)_2\text{O}\cdot\text{H}_2\text{O}$ <sup>8</sup> from

(9) Herrmann, W. A.; Fischer, R. W.; Scherer, W. *Adv. Mater.* **1992**, *4*, 653–658.

(10) (a) Meisel, K. *Z. Anorg. Allg. Chem.* **1932**, *207*, 121–128. (b) Kiprof, P.; Herrmann, W. A.; Kühn, F. E.; Scherer, W.; Kleine, M.; Elison, M.; Rypdal, K.; Volden, H. V.; Gundersen, S.; Haaland, A. *Bull. Soc. Chim. Fr.* **1992**, *129*, 655–662.

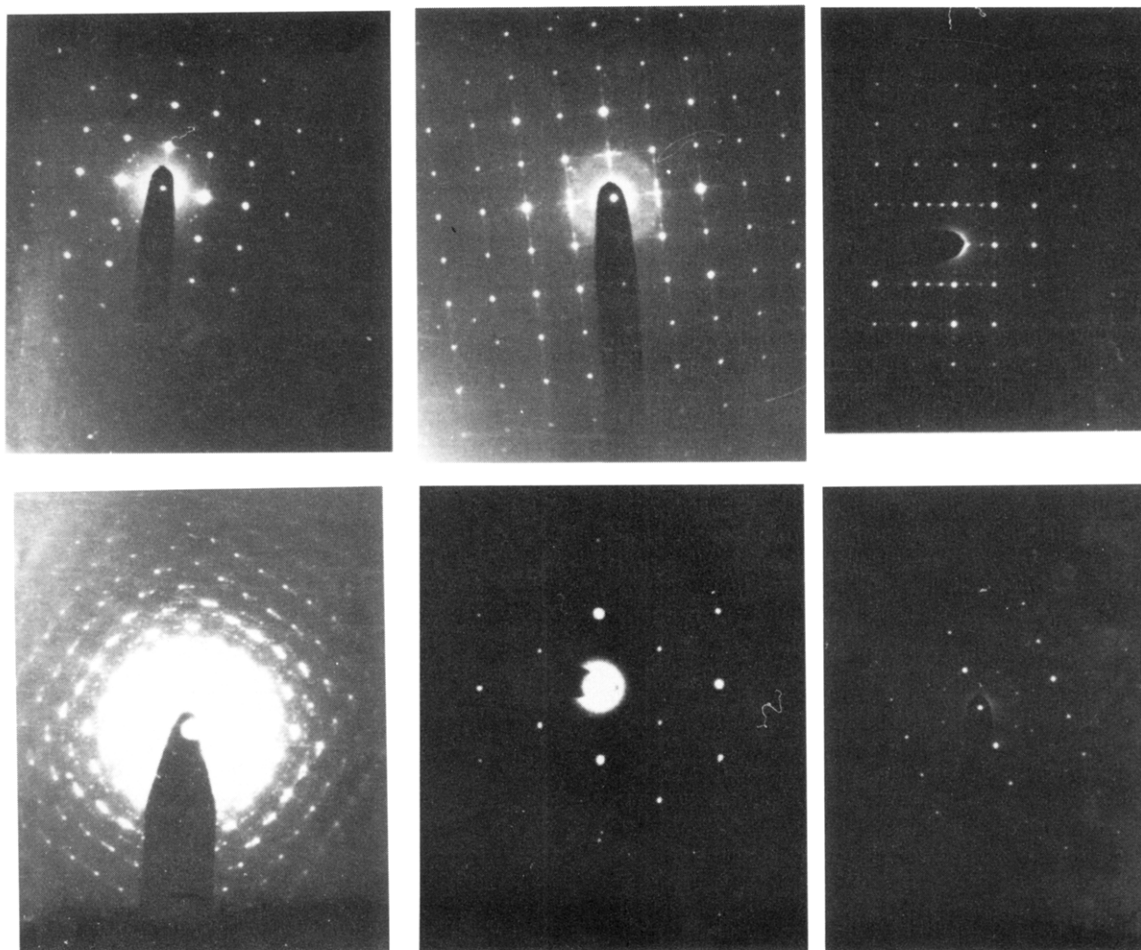


**Figure 5.** Panels are identified as a–f: top row, a–c; bottom row, d–f. (a) Transmission electron diffraction pattern of the reciprocal  $hk0$  plane. The diffraction pattern reveals the square symmetry of the two-dimensional reciprocal lattice which is consistent with the proposed two-dimensional, square space group  $p4mm$ . (b) The diffuse streaks fulfill the same symmetry. (c) Pattern of an orthorhombic modification. (d) Diffraction pattern resulting from twisted two-dimensional crystalline microdomains. (e) Pattern resulting from tilting the crystalline flakes along  $[110]$ . (f) Weakening of all reflections of every second row.

**Table 1.** Crystallographic Data of “poly-MTO” and  $\text{ReO}_3$

	$\{\text{H}_{0.5}[(\text{CH}_3)_{0.92}\text{ReO}_3]\}_\infty$ ( <b>1</b> )	$\text{ReO}_3$
space group	$P4mm^a$	$Pm\bar{3}m$
crystal system	tetragonal <sup>a</sup>	cubic
cell constants	$a = 3.728(1) \text{ \AA}$ $c = 16.516(5) \text{ \AA}^a$	$a = 3.748(1) \text{ \AA}$

<sup>a</sup> The lattice parameter for the third dimension, three-dimensional space group, and crystal system will be derived later (see The Three-Dimensional Model).

“poly-MTO”—based on the fraction of methyl groups—has been observed.<sup>1</sup> Finally, the unusual “depolymerization”  $\mathbf{1} \rightarrow \text{MTO}$  (plus some  $\text{ReO}_3$ ) suggests that the methyl and oxo groups are in a chemical environment similar to that in solid MTO. Monomeric units of MTO were detected when **1** was subjected to the conditions of FT-ICR and FAB mass spectrometry.<sup>1</sup>

While proton NMR spectroscopy of paramagnetic molecular solids is already well established,<sup>11a</sup> the first examination of an organometallic polymer by paramagnetic NMR spectroscopy is presented here. Single-pulse excitation solid-state  $^1\text{H}$  wideline NMR measurement of amorphous **1** in a solenoid probehead yielded the spectrum shown in Figure 7a. Two distinct signals are visible. Both the small line width (2.2 kHz) and the Lorentzian signal shape of the high-field resonance are indicative of protons attached to a highly mobile group. We therefore assign this signal tentatively to the protons of the methyl group which rotates about its 3-fold axis. This assignment is further supported by the chemical shift within the diamagnetic range (0 ppm). The second broad signal (half-width ca. 25 kHz) must

correspond to protons near paramagnetic centers because of the chemical shift at  $\delta = 80$  ppm. The presence of traces of water in the sample cannot be excluded, since both signals are obviously sitting on a broad hump which spans the spectral range from  $-150$  to  $+150$  ppm (the presence and functionality of water will be discussed later). The  $^1\text{H}$  wideline NMR spectrum of a polycrystalline sample of diamagnetic MTO shows a textbook example of dipolar coupling of three spin- $1/2$  nuclei in close proximity (Figure 7b).<sup>11b–d</sup>

Acidic protons have been located by neutron diffraction techniques in related compounds such as  $\text{H}_{0.53}\text{WO}_3$  and  $\text{H}_{1.36}\text{ReO}_3$ .<sup>12</sup> One may postulate that hydrogen in **1** is similarly attached to oxygen atoms of  $\text{Re}-\text{O}-\text{Re}$  bridges. In typical “bronze-type” structures, edge-bridging oxygens are (partially) protonated and O–H bond distances of approximately 100 pm are observed.<sup>12</sup> Terminal oxo groups seem to exhibit less Lewis basicity. For example, the related compound ( $\eta^5\text{-C}_5\text{-Me}_5$ ) $_2\text{Re}_2\text{O}_4$  is protonated only at the oxo bridges and forms also hydrogen bridges at these positions with water;<sup>13</sup>  $\text{CH}_3\text{ReO}_3$  is not protonated even with very strong Brønsted acids.<sup>14</sup> An earlier model<sup>9</sup> which proposed the layers interconnected by

(11) (a) Nayeem, A.; Yesinowski, J. P. *J. Chem. Phys.* **1988**, *89*, 4600. (b) Gutowsky, H. S.; Kistiakowsky, G. B.; Pake, G. E.; Purcell, E. M. *J. Chem. Phys.* **1949**, *17*, 972–981. (c) Richards, R. E.; Smith, J. A. S. *Trans. Faraday Soc.* **1951**, *47*, 1261–1274. (d) Deeley, C. M.; Richards, R. E. *J. Chem. Soc.* **1954**, 3697–3702.

(12) (a) Dickens, P. G.; Weller, M. T. *J. Solid State Chem.* **1983**, *48*, 407–411. (b) Wiseman, P. J.; Dickens, P. G. *Ibid.* **1973**, *6*, 374.

(13) Herrmann, W. A.; Flöel, M.; Kulpe, J.; Felixberger, J. K.; Herdtweck, E. *J. Organomet. Chem.* **1988**, *355*, 297–313.

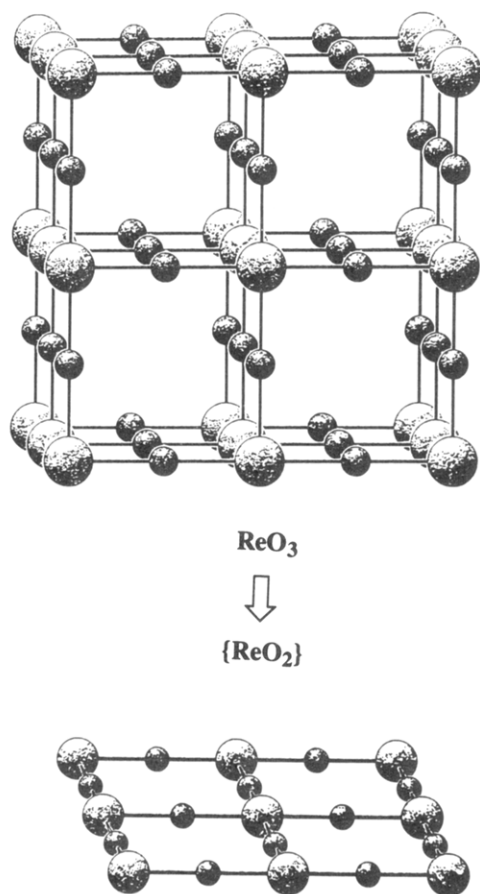


**Figure 6.** Structural comparison of the three-dimensional cubic  $\text{ReO}_3$  network (above) and the two-dimensional square  $\{\text{ReO}_2\}_\infty$  sheets (below).

hydrogen (proton) bridges of type  $\text{Re}=\text{O}\cdots\text{H}^+\cdots\text{O}=\text{Re}$  is not supported by a theoretical treatment of the problem.<sup>15</sup> The molecular orbital calculations indicate that the observed electric conductivity arises from protonation within the  $\text{ReO}_2$  layer.<sup>15</sup>

Since partial demethylation generates a certain concentration of paramagnetic  $\text{Re}^{\text{VI}}$  centers, ESR spectroscopy was also applied.<sup>3</sup> The low-temperature ESR spectra of **1** and  $\text{ReO}_3$  are strikingly similar (322 mT, 9.06 GHz for **1**; 323 mT, 9.05 GHz for  $\text{ReO}_3$ ).  $\text{ReO}_3$  shows one signal without a resolved hyperfine splitting ( $I = 5/2$ ,  $^{185}\text{Re}$  and  $^{187}\text{Re}$ ). The ESR spectrum of the title compound **1** is complex and consists of at least three overlapping signals. Several paramagnetic centers as a result of statistical distribution seem to be present, just as suggested in our structure model. An ESCA study<sup>1,3</sup> also supports the presence of  $\text{Re}^{\text{VI}}$  centers. The latter are responsible for the paramagnetic behavior of **1** at temperatures below 100 K. The temperature dependence of the molar magnetic susceptibility of **1** and  $\text{ReO}_3$  is again very similar.

The  $\{\text{ReO}_2\}_\infty$  framework of Figure 6 gets completed by addition of an oxo and a methyl group, thus resulting in a layer-structure of corner-sharing  $\text{ReO}_5(\text{CH}_3)$  octahedra. This structural model adopts the three-dimensional extended  $\text{ReO}_3$  motif in two dimensions as a  $\{\text{ReO}_2\}_\infty$  network (Figure 8).

The  $\text{Re}-\text{C}$  and  $\text{Re}=\text{O}$  bond distances should be slightly longer than those of (monomeric) MTO ( $\text{Re}=\text{O}$ , 1.702(2) Å;  $\text{Re}-\text{C}$ , 2.063(2) Å; Figure 2) since reduction by the extra hydrogen equivalents has occurred. The  $\text{Re}\cdots\text{Re}'$  distance is identical with the cell constant  $a = 3.728(1)$  Å. There is no

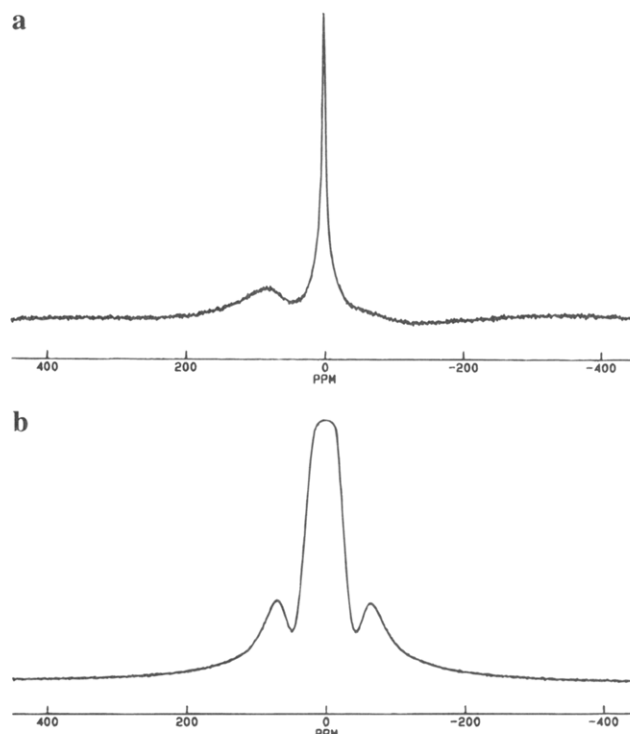


**Figure 7.** 300 MHz wide-line  $^1\text{H}$  NMR spectra obtained by single-pulse excitation. (a) “Poly-MTO” (**1**) (3000 transients). The narrow signal at low frequency corresponds to methyl groups and the high-frequency broad signal to protons near paramagnetic centers. (b) Polycrystalline MTO (4000 transients). Resonance of methyl protons, for details see text.

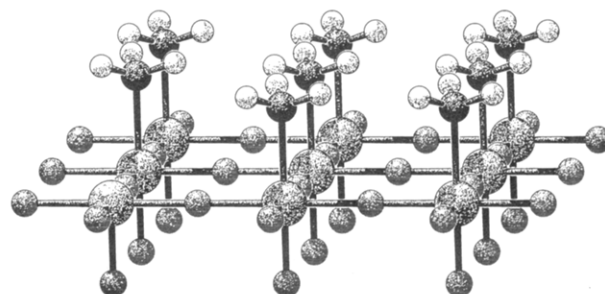


**Figure 8.** Idealized two-dimensional model of the layer-structure of corner-sharing  $\text{ReO}_5(\text{CH}_3)$  octahedra. Four square unit cells are drawn. The positions of the acidic protons are not indicated since they are statistically distributed across the  $\{\text{ReO}_2\}_\infty$  planes. The positions of methyl-free rhenium ( $\text{Re}^{\text{VI}}$ ) are also statistically arranged. According to the analytical composition of **1**, ca. 8% of the original methyl groups are lost during formation of **1** from MTO in water.<sup>1,3</sup> One demethylated rhenium site is indicated by a shaded circle in the first of the four unit cells.

evidence as to the geometry of these  $\text{Re}-\text{O}-\text{Re}$  bridges, e.g. whether they are linear or not. In related systems, such as  $\text{H}_{0.53}\text{WO}_3$  and  $\text{H}_{1.36}\text{ReO}_3$ ,<sup>12</sup> the  $\text{M}-\text{O}-\text{M}$  units ( $\text{M} = \text{W}, \text{Re}$ ) are slightly bent (ca.  $170^\circ$ ) as they get protonated to give  $\text{M}-(\text{OH})-\text{M}$  moieties. In addition, there are no experimental data available to assign the “tacticity” (up or down) of the methyl vs oxo pattern in the structural model of **1** (Figure 8).

We propose a disordered model in which methyl-free rhenium(VI) sites are completely statistically distributed over the entire  $\{\text{ReO}_2\}_\infty$  network to explain the diffuse streaks along  $a^*$  and  $b^*$  in the electron diffraction pattern (Figure 5b). The sharp Bragg reflections result from positions of the rhenium atoms alone. These heavy atoms are the dominant scattering centers in the model. Their positions are obviously not much affected by the disorder problem. In one case, however, we could find another type of crystal showing sharp reflections

(14) Herrmann, W. A. *Angew. Chem.* **1988**, *100*, 1269–1286; *Angew. Chem., Int. Ed. Engl.* **1988**, *10*, 1297–1313.

(15) Genin, H. S.; Lawler, K. A.; Hoffmann, R.; Herrmann, W. A.; Fischer, R. W.; Scherer, W. *J. Am. Chem. Soc.* **1995**, *117*, 3244.

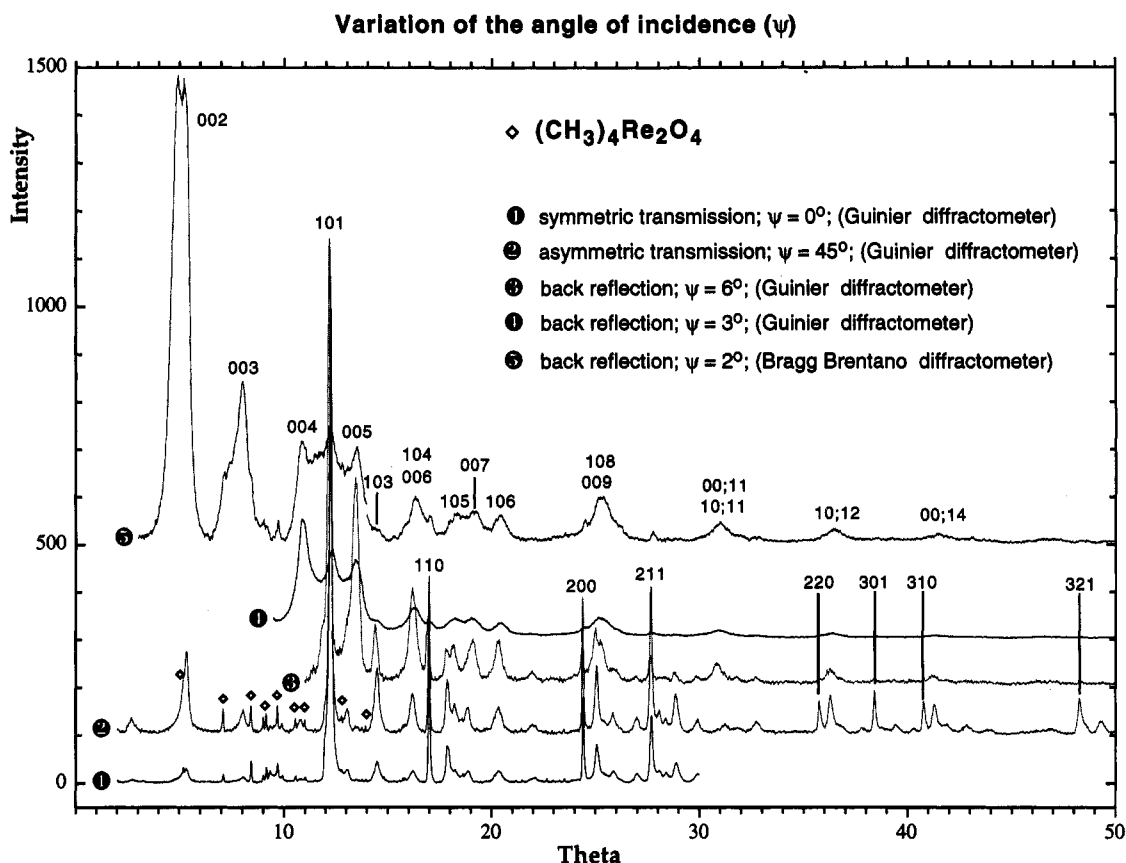


**Figure 9.** X-ray diffraction pattern of moist "poly-MTO" (1). The five samples were measured at different angles of incidence (see the Experimental Section). Reflections originating from single-crystalline  $(\text{CH}_3)_4\text{Re}_2\text{O}_4$ <sup>4,20</sup> are marked in pattern 2. (Single crystals of  $(\text{CH}_3)_4\text{Re}_2\text{O}_4$  were not removed by washing raw "poly-MTO" samples with THF because such a washing procedure decreases the degree of crystallinity of the sample.)

along (at least) one main direction of the reciprocal lattice (Figure 5c). The structure of this crystalline particle belongs to the orthorhombic system. The lattice constants calculated from this pattern are  $a = 3.81$  and  $b = 11.16$  Å ( $b = 3a$  within the accuracy of measurement). The ordering along the crystallographic axes in Figure 5c is obviously different from that in Figure 5a, causing the observed tripling of (at least) one lattice constant. This superstructure effect might be a consequence of the distortion of the  $\text{ReO}_5(\text{CH}_3)$  groups away from perfect octahedra as result of *bent* M–O–M units. As mentioned above, the M–(OH)–M units of  $\text{H}_{0.53}\text{WO}_3$  and  $\text{H}_{1.36}\text{ReO}_3$ <sup>12</sup> are also slightly bent. In these cases the distortion of the  $\text{MO}_6$  octahedra resulted in a doubling of the lattice constants of the cubic cell.

### The Three-Dimensional Model—A Double-Layer Structure with Intercalated Water

Up to now we solely concentrated on electron diffraction experiments on nearly completely dehydrated "poly-MTO" (1) under high-vacuum conditions. These samples result from extensive washing and drying procedures.<sup>3</sup> In the X-ray powder diffraction experiments of 1, additional diffuse and broad reflections could be observed besides the  $hk0$  reflections (see above). These reflections gain intensity and narrow to smaller peak half-widths if moist samples of raw poly-MTO (1) (from aqueous suspensions and *without drying* under high-vacuum conditions) are recorded. Some of the additional peaks become the dominant peaks in the pattern (Figure 9) when measurements were carried out at small angles of incidence ( $2$ – $6^\circ$ ), thus being identified as the missing  $00l$ -reflection series of "poly-MTO". The complete diffraction pattern could now be indexed on the basis of a tetragonal unit cell:  $a = 3.728(1)$ ;  $c = 16.516(5)$  Å (space group  $P4mm$ ). Similar cell constants could also be found

for inorganic bronze-type structures, e.g.  $\text{H}_x\text{MO}_3$ ,<sup>16a</sup> which consists of two-dimensional double layers of face-sharing  $\text{MO}_3$  octahedra. Assuming two layers of "poly-MTO" per unit cell leads to an average interlayer distance of 8.22 Å, which is compatible with *one additional intercalated water layer*.

The diffraction pattern of the water intercalation modification of 1 shows a weakening of *all*  $hkl$  reflections with  $h + k + l$  odd, implying a *nearly body-centered unit cell* with a *staggered* arrangement of the individual "poly-MTO" layers. Due to the centering the  $hk0$  reflections 100, 210, 300, and 320 (present in the electron diffraction pattern of 1) are absent in the case of 1 while high intensities for the corresponding  $hkl$  reflections (101, 211, 301, and 321) are observed. By way of contrast the  $00l$  reflections only show a weakening for the 001, 003, and 005 reflections. Obviously the body centering is nearly perfect regarding the  $a$  and  $b$  axes of the unit cell but not completely fulfilled along the  $c$  axis. This can be explained by a model in which the "poly-MTO" layer ( $A'$ ) (being displaced by  $(a + b)/2$  relative to  $A$ ) should have *two different interlayer distances* toward both adjacent layers ( $A$ ) with a resulting layer sequence of  $A-A'-A-A'$ ...

We propose that the two different interlayer distances of about 7.4 and 9.1 Å result from a layer arrangement in which the oxo groups of two adjacent layers are *vis-à-vis* (Figure 10), with a water layer (B) intercalated between the oxo groups of adjacent layers and a layer sequence of  $ABA'AB$ ... This model allows the formation of hydrogen bridges between the water molecules and the oxo groups of adjacent "poly-MTO" double layers. *The water molecules therefore play a dominant role in connecting such double layers.* The observed loss of crystal-

(16) (a) Schröder, F. A.; Weitzel, H. *Z. Anorg. Allg. Chem.* **1977**, *435*, 247–256. (b) Schlemper, E. O.; Hamilton, W. C. *Inorg. Chem.* **1966**, *5*, 995–998. (c) Jeitschko, W.; Sleight, A. W. *J. Solid State Chem.* **1972**, *4*, 324–330.

linity in vacuum-dried samples of **1** and the pronounced hygroscopicity of such samples thus finds a simple explanation in the important structural function of the intercalated water molecules. The unpolar methyl groups are oriented inside the double layer. The double layers are therefore interconnected by *van der Waals* attractions which are in agreement with the observed high lubricity of “poly-MTO”.

Interconnecting water layers of this kind are known for layer structures of clay minerals, e.g. montmorillonite. The unit cell of fully hydrated **1** comprises a close packing of the “poly-MTO” and water layers, so there is no space left for additional solvent molecules. (Only holes of about  $8 \text{ \AA}^3$  in size are present, assuming water molecules centered at  $00z$  (Figure 10) and resulting in a maximum amount of one water molecule per two “ $\text{CH}_3\text{ReO}_3$ ” units.) However, the packing of corner-sharing  $\text{CH}_3\text{ReO}_5$  octahedra in **1** seems energetically less favored as compared to the “isolated”, and close-packed tetrahedra of  $\text{CH}_3\text{-ReO}_3$  in the structure of MTO. It is thus no longer surprising that “poly-MTO” undergoes “depolymerization” under various conditions.<sup>1,3</sup>

It was noted above that the intensities of the  $hk0$  reflections increase with increasing angle of incidence (Figure 9). This phenomenon indicates a preferred orientation of the crystalline flakes along the surface of the sample holder. The same is true for the recorded intensities of the  $00l$  reflections: they increase with decreasing angle of incidence, in full agreement with such a preferred orientation (Figure 9).

Different peak half-widths for different classes of reflections are also observed: the  $hk0$  reflections are much narrower than the  $00l$  and  $hkl$  reflections. This anisotropic broadening might arise from lattice distortion and disorder problems (e.g., defect broadening due to partial dehydration of **1**) along the third crystal dimension or simply from a size effect due to nanoscale thickness of the layers. In addition, a polytypism effect due to alternative stacking arrangements of the water and “poly-MTO” layers could be responsible for the observed anisotropic broadening.

The calculated and observed X-ray diffraction patterns (ignoring the preferred orientation and the disorder problems) are shown in Figure 11. A neutron diffraction study is expected to improve and refine the structure of **1**.<sup>17a</sup>

**(a) Checking the Local Symmetry by Infrared and FT-Raman Spectroscopy.** The infrared spectra of **1**,<sup>9</sup> of fully deuterated **1**,<sup>9</sup> and of MTO<sup>1,18</sup> have been discussed and compared in detail. To check the local symmetry of the suggested three-dimensional structure model, we recorded a FT-Raman spectrum of **1**.

A factor group analysis was performed using Adams and Newton tables<sup>19</sup> for the  $P4mm$  crystallographic space group. In case of  $Z = 2$  molecules per primitive unit cell, the most characteristic  $\text{Re}=\text{O}$  and  $\text{Re}-\text{C}$  “axial”-stretching modes show  $2A_1$  and  $B_1$  modes. The observed spectra are consistent with the results of factor group analysis: the  $B_1$  modes are only Raman active while the  $A_1$  modes are active in both the Raman and IR spectra (Figure 12). According to the above selection rules, three bands ( $2A_1 + B_1$ ) were always observed in the Raman spectra, and there are only two bands in the infrared ( $2A_1$ ) that coincide with the Raman frequencies. In case of MTO, only *one*  $\text{Re}-\text{C}$  stretching mode ( $A_1$ ) is observed at 572

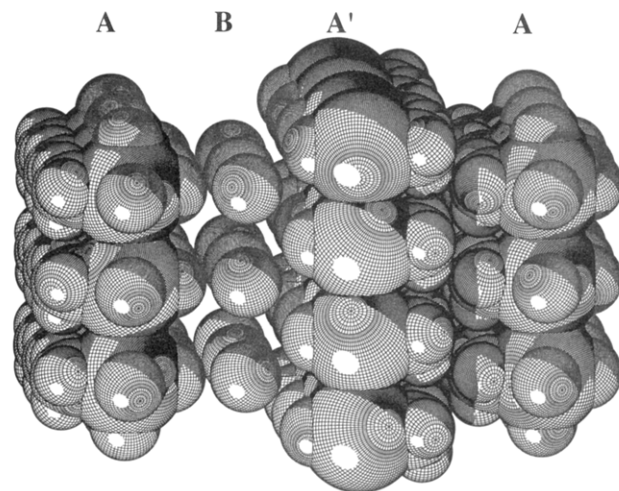


**Figure 10.** Suggested, idealized structure model of “poly-MTO” (**1**,  $\{\text{H}_{0.5}[(\text{CH}_3)\text{ReO}_3](\text{H}_2\text{O})_{0.5}\}_\infty$ ) (space-filling model).

and  $576 \text{ cm}^{-1}$  (IR and Raman spectra, respectively) in the solid state. As can be judged from the average position of the  $\nu$ -( $\text{Re}=\text{O}$ ) bands, the rhenium–oxygen bond strength is less than in MTO, for which the  $\text{Re}=\text{O}$  force constant is calculated at  $8.15 \text{ N}\cdot\text{cm}^{-1}$ .<sup>18</sup> A simplified calculation for “poly-MTO” gives  $7.34 \text{ N}\cdot\text{cm}^{-1}$ . Slightly longer  $\text{ReO}$  bond distances in “poly-MTO” vs MTO ( $1.702 \text{ \AA}$ ) are thus reasonable to assume and in agreement with our suggested model (Figure 10, Table 2).

The site symmetries of the rhenium position in **1** and  $\text{ReO}_3$  are related by a group–subgroup relationship:  $O_h (\text{ReO}_3) \rightarrow D_{4h} \rightarrow C_{4v} (\mathbf{1})$ . Due to the higher site symmetry in the case of  $\text{ReO}_3$ , only *one* IR-active  $\text{Re}=\text{O}$  stretching mode ( $F_{1u}$ ) is observed ( $913 \text{ cm}^{-1}$ ). In the case of MTO only *one*  $\text{Re}-\text{C}$  stretching mode ( $A_1$ ) at  $572$  and  $576 \text{ cm}^{-1}$  (IR and Raman spectra, respectively) can be recorded (site symmetry for the rhenium position is  $C_s$ ).

**(b) Further GED Investigations of Partially Amorphous Domains of **1**.** The electron diffraction experiments were performed on partially dehydrated “poly-MTO” (**1**) due to the high-vacuum conditions necessary for such experiments. The X-ray diffraction patterns of such samples show very broad  $00l$  reflections. The same is true for the electron diffraction patterns of **1**—they do not yield a resolved three-dimensional reciprocal lattice: no  $hkl$  or  $00l$  reflections were detected. *Nevertheless the  $00l$  reflections are still present* because the electron diffraction pattern (Figure 5a) does not change very much upon tilting the goniometer except a little bit for the distances perpendicular to the tilt axis and the angles between the rows of reflections. The reciprocal space construction for such a two-dimensional diffraction consists of spread diffuse  $00l$  rods parallel to  $c^*$  (Figure 13). Such diffuse  $00l$  rods correspond to the observed broad diffuse reflections in the X-ray diffraction pattern of **1** dried by standard procedures (high vacuum). A projection along  $c^*$  results in the observed two-dimensional diffraction pattern of the reciprocal  $hk0$  plane (Figure 5a). In one case, we also could observe the diffraction pattern shown in Figure 5e: this pattern results from extreme tilting of the crystalline flake along  $[110]$ , and it is also in agreement with the proposed reciprocal space construction (Figure 13).

This effect is indicative for a strongly disordered stacking of such layers (either parallel to  $a$ ,  $b$ , or  $c$ ) and is supported by a size effect due to nanoscale thickness of the layers. So far none of the crystals (about  $2 \mu\text{m}$  in diameter) could be imaged under high-resolution conditions because they rapidly deteriorated on increasing the intensity of the electron beam. Obviously the thickness of these crystalline flakes escapes our determination. However, we assume a nanoscale thickness of only a few unit

(17) (a) A study is underway at the Rutherford Appleton Laboratory (ISIS), Chilton, Didcot, Oxon OX110QX, Great Britain. (b) Cockcroft, J. K. Profil (V. 5.12), a Rietveld Refinement Program with Chemical Constraints, Institut Laue-Langevin, Grenoble, France.

(18) Mink, J.; Stirling, A.; Keresztury, G.; Herrmann, W. A. *Spectrochim. Acta* **1994**, *50A*, 2039.

(19) Adams D. M.; Newton, D. C. *Tables for Factor Group and Point Group Analysis*; Beckman-RIC Ltd.: Sunley House, 4 Bedford Park, Croydon CR9 3LG, England, 1970.

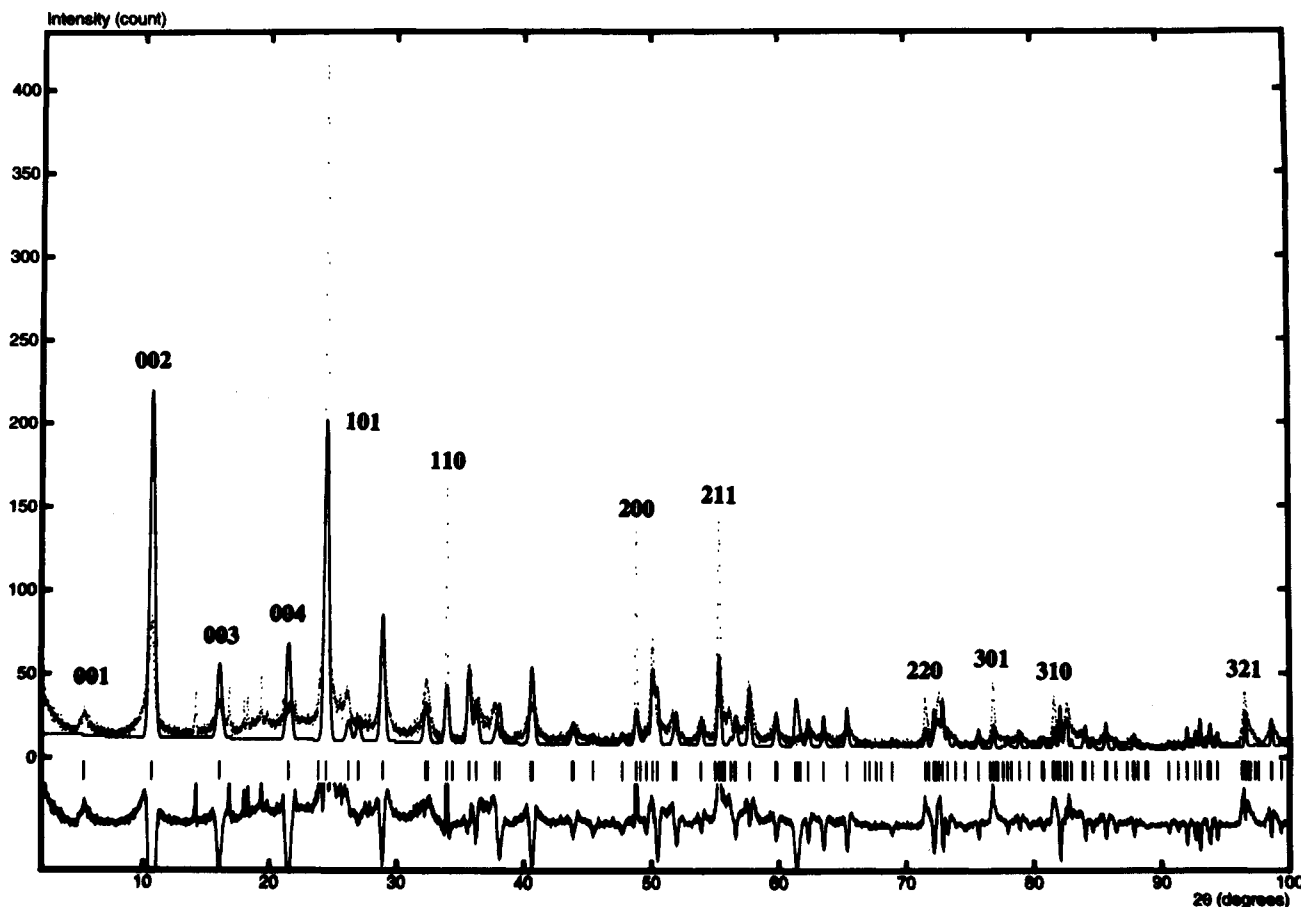


**Figure 11.** Calculated and observed diffraction pattern of hydrated “poly-MTO” (**1**,  $\{H_{0.5}[(CH_3)ReO_3](H_2O)_{0.5}\}_\infty$ ) (without correction of the preferred orientation and anisotropic broadening; extra spots are originating from  $(CH_3)_4Re_2O_4$ ;<sup>20</sup> see Figure 9; pattern 2. Only the scale factor, the lattice, and instrumental parameters ( $2\theta$  zero point displacement,  $V$ ,  $W$ ) were refined with fixed atomic positions.<sup>17b</sup>

cells due to the high transparency of the observed crystalline flakes. Suspensions of the substance in water thus favor separation and preferred orientation of the “poly-MTO” layers on the support grid, resulting in the usually observed diffraction pattern of Figure 5a. The same preferred orientation phenomenon has been observed in the X-ray diffraction experiments (see above). SEM and a TEM images of sedimented “poly-MTO” flakes nearly aligned along the surface of the sample holder are shown in Figure 14, parts a and b, respectively.

Diffraction patterns of such overlapping “twisted layers” as shown in Figure 5d are to be interpreted as powder patterns that still show only resolved  $hk0$  reflections. In no case were resolved  $00l$  reflections observed. This demonstrates again that the presence of water plays an important role for the three-dimensional order in “poly-MTO”. Nevertheless indications of a third dimension are seen in one case (Figure 5f): every second row of reflections is weakened here, with the layers obviously not being twisted but rather systematically translated along one crystallographic main direction (approximately half the lattice constant).

**(c) Model for the Amorphous Domains of 1.** Up to now all diffraction experiments were dealing with the crystalline (hydrated) or partially crystalline (partially dehydrated) domains of **1**. This investigation shows that the crystallinity and the ordering of the “poly-MTO” layers is strongly influenced by the amount of water. However, it cannot be concluded from these results that the amorphous bulk domains of **1** do not exhibit any kind of interlayer ordering. If one considers a simple three-dimensional model of *eclipsed* layers of corner-sharing  $ReO_5$ - $(CH_3)$  octahedra (TlAlF<sub>4</sub>-type), an average interlayer distance of about 6.8 Å is calculated from the observed density ( $\rho = 4.38 \text{ g cm}^{-3}$ ). This distance is consistent with theoretical calculations,

according to which interlayer distances smaller than 6 Å imply a significant destabilization due to *van der Waals* repulsions between individual layers.<sup>15</sup> Such an eclipsed model is compatible with the tetragonal unit cell (see above). An alternative, staggered packing of adjacent layers is represented by a  $SnF_4/(CH_3)_2SnF_2$ <sup>[16b]</sup>-type model.

We explain the lack of pronounced ordering along the third dimension in the amorphous domains by the complete lack of intercalated water molecules and therefore by small interlayer interactions and variable interlayer distances originating from more or less statistically alternating (“atactic”) methyl and oxo group positions.

**(d) Quantification of the Water Content in 1 by TGA-MS Investigations.** It is important to stress that the empirical formula  $\{H_{0.5}[(CH_3)_{0.92}ReO_3]\}_\infty$  accounts for samples prepared under standard conditions (washing with water, ether, THF, and pentane and drying under high-vacuum conditions). Nevertheless, careful inspections of the TGA-MS measurements reveal that also in these samples traces of water are still present. This is in agreement with the observed X-ray diffraction pattern which shows also for such vacuum-dried samples  $00l$  reflections indicative of the water layer. Also the IR spectra<sup>3</sup> and the solid-state <sup>1</sup>H NMR spectra (discussed above) are in agreement with the assumption that traces of water are inherently present in **1**. The presence of water has been taken into consideration in the new formula for **1**:  $\{H_{0.5-2x}[(CH_3)_{0.92}ReO_{3-x}](H_2O)_x\}_\infty$ .

**Quantification of “x” by TGA-MS Investigations.** Samples of **1** (freshly synthesized in D<sub>2</sub>O and “dried” under high-vacuum conditions (turbo-pump coupled with MS, 10<sup>-5</sup> Torr)) show even after 3 days a significant D<sub>2</sub>O signal ( $m/z = 20$ ). To quantify the amount of intercalated water, we performed TGA-

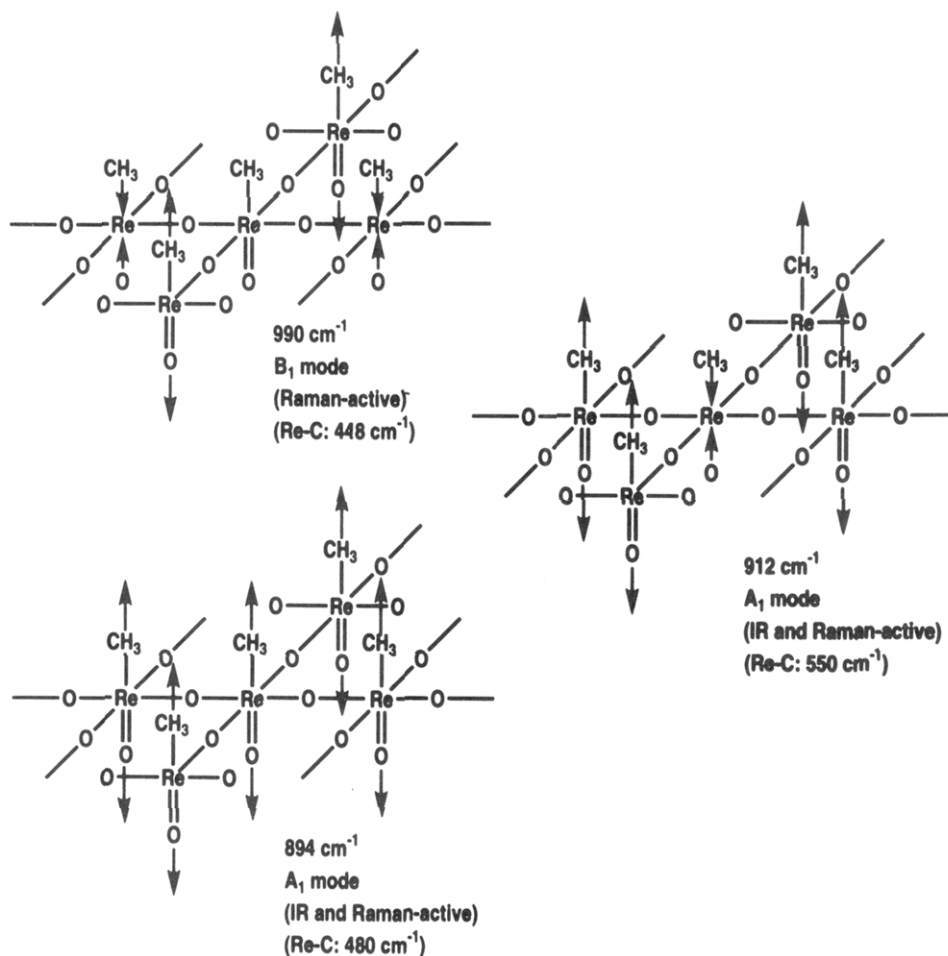


Figure 12. Re=O and Re-C stretching modes in "poly-MTO", see text.

MS experiments (see Experimental Section). They show that the amount of intercalated water should be smaller than 2 wt %:  $\bar{x} < 0.29$ . The TGA-MS results correspond to an average value  $\bar{x}$  for the bulk sample.

**Quantification by Stoichiometry.** The amount of "extra hydrogen atoms" in  $\{\text{H}_{0.5}[(\text{CH}_3)_{0.92}\text{ReO}_3]\}_\infty$  provides the upper limit of the water content:  $\bar{x}_{\text{max}} = 0.25$ . This upper limit is in agreement with the experimental value in the range of the systematic limitations of both methods: elemental analysis and TGA-MS. The water and the acidic protons are detectable simultaneously by the solid-state NMR experiment, so  $\bar{x}$  should be smaller than this stoichiometric limit:  $\bar{x} < 0.25$ .

**Crystallographic Considerations.** Assuming the water molecules are located at  $00z$ , only "holes" of about  $8 \text{ \AA}^3$  in size are present in the unit cell. Therefore no space is left for additional water molecules and therefore an ideal value of  $x_{\text{ideal}} = 0.5$  should be the upper limit for completely hydrated samples of **1**. At this stage it is important to stress that not the crystalline but the amorphous domains constitute the dominant part of **1**. Therefore, we still can assume a value of  $x = 0.5$  for the crystalline portions of **1** and the value of  $\bar{x} < 0.25$  will still be valid for both domains (amorphous and crystalline).

For the partially amorphous areas we propose a model with turbostratic and  $00l$  defect stacking of the double layers of corner-sharing  $\text{ReO}_5(\text{CH}_3)$  octahedra (see above). In these areas we expect a much lower value of  $x$  than in the crystalline areas resulting in an all over value of  $\bar{x} \ll 0.25$  (Figure 15).

It has to be stressed that the interlayer separation in **1** (Figure 10) does not vary as a function of  $x$ . We showed that *the intercalated water can hardly be removed* by drying procedures under high-vacuum conditions. This accounts for the observa-

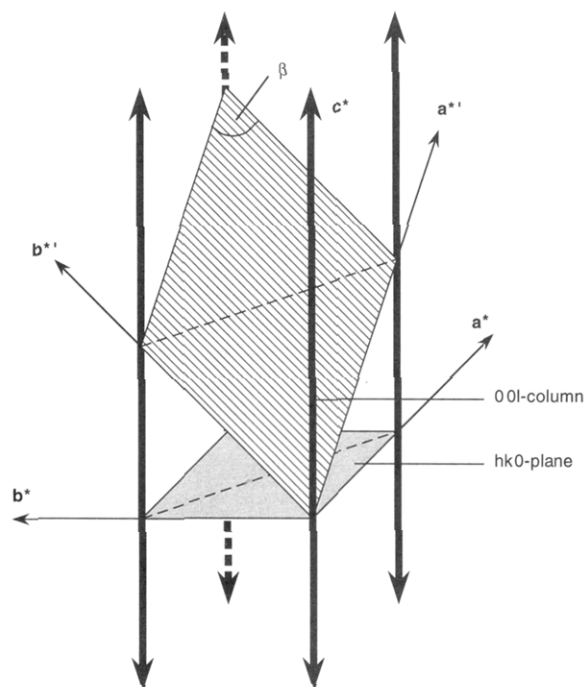
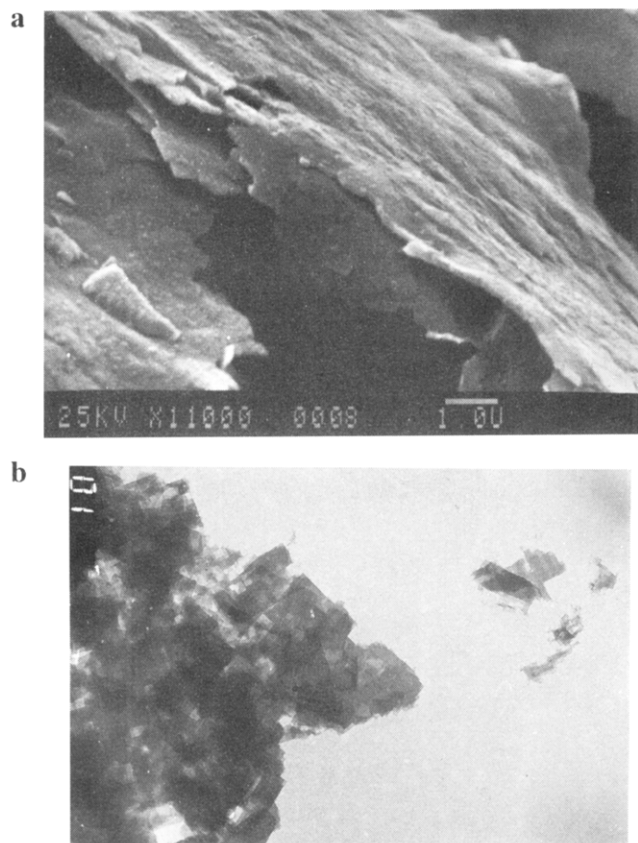


Figure 13. Reciprocal space construction. All reciprocal spots are spread out to form diffuse rods. Tilting of these thin layers leads to distortions of the square reciprocal lattice toward a "rhombic" reciprocal lattice.

tion that there are always crystalline domains in **1** with intact water layers.



**Figure 14.** SEM micrograph (top, 11 000 $\times$  magnification) and TEM micrograph (bottom, 25 000 $\times$  magnification) of "sedimented flakes" of "poly-MTO" (**1**).

The vacuum drying procedure simply reduces the portions of the hydrated, crystalline areas but does not affect the interlayer distance of the remaining hydrated areas. This is in agreement with the observation that only the peak half-widths of the 00 $l$  reflections are affected by the drying procedure (due to the loss of crystallinity) while the  $d$ -values remain invariant.

It has also to be emphasized that values of  $x > 0$  cause a small understoichiometry with respect to the Re/O ratio (1:3). We therefore cannot exclude that small amounts of amorphous  $\text{ReO}_2$  are present in the bulk domains of **1** which account for this understoichiometry. ( $\text{Re}^{\text{IV}}$  centers have been determined for **1** by ESCA, but they could be also generated by the experimental conditions.)<sup>3</sup>  $\text{Re}^{\text{IV}}$  centers inside the "poly-MTO" layers are unlikely and would suggest Re atoms lacking both the methyl and a terminal oxo group. Up to now  $\text{Re}^{\text{IV}}$  centers in rhenium bronzes have only been observed for the high-pressure modification of  $\text{ReO}_3$ : the golden-colored  $\text{Re}_{1.16}\text{O}_3$ .<sup>16c</sup>

## Conclusion

"Poly-MTO" is the first example of a polymeric organometallic oxide. The structure of the crystalline domains of **1** is best described by double layers of corner-sharing  $\text{CH}_3\text{ReO}_5$  octahedra (AA') with intercalated water molecules (B) (AA'BAA'... layer sequence). The oxo groups of two adjacent layers are vis-à-vis (Figure 10), with a water layer (B) intercalated between the oxo groups of adjacent layers. This model allows the formation of H-bridges between the water molecules and the oxo groups of adjacent "poly-MTO" double layers. *The water molecules therefore play a dominant role in connecting such double layers.* The observed loss of crystallinity in vacuum-dried samples of **1** and the pronounced hygroscopicity of such samples thus find a simple explanation. The unpolar methyl groups are oriented inside the double layer.

The double layers are therefore interconnected by *van der Waals* attractions in agreement with the observed remarkable lubricity of "poly-MTO". High electric conductivity results from understoichiometry with respect to the  $\text{CH}_3/\text{Re}$  ratio (9.2/10) and partial reduction by extra hydrogen equivalents.

For the amorphous areas, we propose a model with turbostratic and 00 $l$  defect stacking of the double layers of corner-sharing  $\text{ReO}_5(\text{CH}_3)$  octahedra with smaller water contents.

As compared to the classical  $\text{ReO}_3$ -type structure, an additional  $\text{CH}_3$  group present in **1** cannot act as a bridging ligand and connect adjacent layers. However, if this extra ligand eliminates under thermal or photochemical conditions, only small structural changes are necessary to transform the layer-type polymeric organometallic oxide **1** into the three-dimensional metal oxide  $\text{ReO}_3$ . This aspect of organometallic chemistry is new and warrants further exploration, e.g. in the formation of three-dimensional mixed perovskites by the introduction of  $\text{ReO}_3$ .

## Experimental Section

Information concerning other analytical and chemical studies is summarized in the chemical part of this publication<sup>1</sup> and in a thesis.<sup>3</sup>

**(1) X-ray Powder Diffraction.** Powder diffraction patterns of **1**,  $\text{ReO}_2$ ,  $\text{ReO}_3$ ,  $\text{NH}_4\text{ReO}_4$ ,  $\text{CH}_3\text{ReO}_3$ ,  $(\text{CH}_3)_4\text{Re}_2\text{O}_4$ , and  $(\text{CH}_3)_6\text{Re}_2\text{O}_5$  were recorded using varying measuring conditions on three Guinier diffractometers supplied by HUBER with Ge or Si monochromators ( $\lambda = 154.056$  pm) and computer-controlled single-channel NaI scintillation detectors. The data were collected with counting times and step widths in the range of  $t = 2\text{--}20$  s and  $\theta = 0.002\text{--}0.01^\circ$  (step-scanning method).

**(a) "Poly-MTO".** Samples of "poly-MTO" (**1**) were studied in both symmetric and asymmetric transmission geometries on a G642 Guinier diffractometer for flat powdered samples. Samples of **1** were ground in an agate mortar and strewn on a foil (thickness  $< 0.02$  mm) that was covered with a thin film of Vaseline. The diffraction patterns were found to be nearly independent of the grinding time. Obviously the dimensions of the crystalline nanoflakes are too small to be much influenced by common grinding procedures. Thin films of **1** (dried aqueous suspensions) were also studied on thin polypropylene foils.

Measurements at different angles of incidence ( $\Psi = 2\text{--}6^\circ$ ) were recorded on a Huber G642 Guinier diffractometer (symmetric transmission, angle of incidence  $\alpha = 90^\circ$ ; asymmetric transmission,  $\alpha = 45^\circ$ ), in back-reflection on a G653 Guinier thin-film diffractometer ( $\alpha = 3\text{--}6^\circ$ ), and also on a Siemens D5000 diffractometer ( $\alpha = 2^\circ$ ).

Crystallographic data of "poly-MTO" (hydrated form) are as follows: tetragonal,  $P4mm$  (Int. Tab. No. 99),  $a = 3.728(1)$  Å,  $c = 16.516(5)$  Å. In the X-ray diffraction pattern of raw "poly-MTO" samples, extra peaks belonging to the well-known dimeric compound  $(\text{CH}_3)_4\text{Re}_2\text{O}_4$ <sup>20</sup> (less than 4% by analysis) were detected by means of X-ray diffraction (powder and single-crystal methods). This compound exhibits two bridging oxo ligands. This "impurity" can be removed by washing samples of "poly-MTO" with water, diethyl ether, and THF. After this washing procedure, only the X-ray powder pattern of the title compound is present.

**(b)  $\text{ReO}_2$ .** Dry samples of "poly-MTO" (**1**) were ground in an agate mortar and sealed in thin quartz capillaries (0.5 mm i.d.; all operations performed in a glovebox). The capillaries were rotated continuously during heating and measuring (temperature range, 25–400 °C;  $\Delta T/\text{scan}$ , 25 °C; counting times, 20 s; step widths,  $\theta = 0.02^\circ$ ; measuring interval,  $\theta = 8\text{--}18^\circ$ ) on a G644 Guinier diffractometer equipped with a heating unit). The sample was tempered at 400 °C for 10 h, and afterwards, the diffraction pattern of  $\text{ReO}_2$  (measuring interval of  $\theta = 2\text{--}50^\circ$ ) was recorded at room temperature: orthorhombic space group  $Pbcn$  (no. 60),  $a = 4.806(2)$  Å,  $b = 5.631(4)$  Å,  $c = 4.623(2)$  Å.

**(c)  $\text{ReO}_3$ .** Raw samples of "poly-MTO" (**1**) were ground in an agate mortar and sealed in thin quartz capillaries (0.3–0.5 mm i.d.). The capillaries were rotated continuously during heating and measuring (temperature range, 25–400 °C;  $\Delta T/\text{scan}$ , 25 °C; counting times, 10 s; step widths,  $\theta = 0.01^\circ$ ; measuring interval, 8–20° on a G644 Guinier

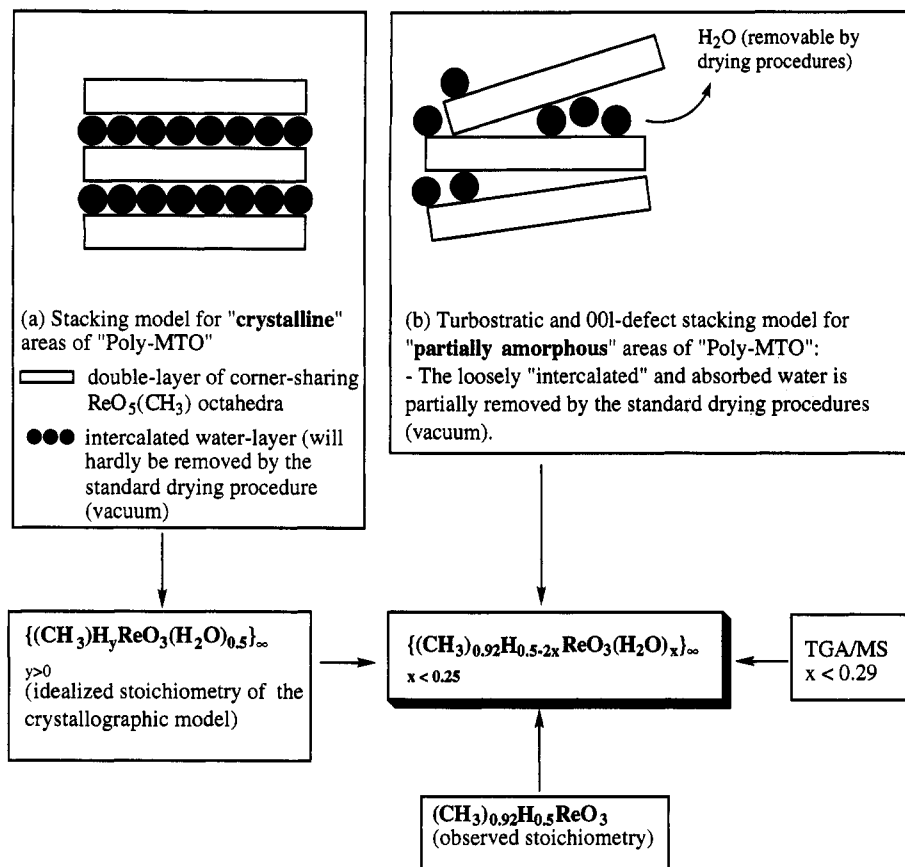


Figure 15. Quantification of "x" in  $\{\text{H}_{0.5-2x}(\text{CH}_3)_{0.92}\text{ReO}_3-x(\text{H}_2\text{O})_x\}_\infty$  (1).

Table 2. Coordinates of the Suggested and Idealized Structure Model of "Poly-MTO":<sup>a</sup>  $\{\text{H}_{0.5}(\text{CH}_3)\text{ReO}_3(\text{H}_2\text{O})_{0.5}\}_\infty$

atom	$x/a$	$y/b$	$z/c$
Re1	0	0	0
O1	$1/2$	0	0
O2	0	0	-0.106 40
C1	0	0	0.130 80
H1	0.171 50	0.171 50	0.151 40
H2	0.062 80	-0.234 20	0.151 40
H3	-0.234 20	0.062 80	0.151 40
Re2	$1/2$	$1/2$	0.448 00
O3	$1/2$	0	0.448 00
O4	$1/2$	$1/2$	0.554 40
O5	0	0	0.725 10
C2	$1/2$	$1/2$	0.317 20
H4	0.671 50	0.671 50	0.296 60
H5	0.562 80	0.265 80	0.296 60
H6	0.265 80	0.562 80	0.296 60

<sup>a</sup> The local symmetry of the  $\text{CH}_3$  group does not fulfill the local crystallographic symmetry of  $4mm$ ; thus, the hydrogen positions are disordered. The positions of acidic protons and the hydrogen atoms of the water molecule are not included in the structure model.

diffractometer equipped with a heating unit). The diffraction pattern of  $\text{ReO}_3$  (measuring interval of  $\theta = 2-50^\circ$ ) was obtained at room temperature: cubic space group  $Pm\bar{3}m$  (no. 221),  $a = 3.748(1)$  Å.

(d)  $\text{NH}_4\text{ReO}_4$ . The diffraction patterns of "poly-MTO" (1) samples were recorded in asymmetric transmission geometry on a G642 Guinier diffractometer in "step-scanning mode" (counting times, 10–20 s; step widths,  $\theta = 0.005-0.01^\circ$ ; measuring interval,  $\theta = 2-50^\circ$ ). After 2 days, the first weak reflections originating from  $\text{NH}_4\text{ReO}_4$  were detected. After 4 weeks, no "poly-MTO" reflections at all could be detected. Only very small reflections from single-crystalline, colorless prisms of  $\text{NH}_4\text{ReO}_4$  appeared in the diffraction pattern: tetragonal space group  $I4_1/a$  (no. 88);  $a = 5.883(1)$ ,  $c = 12.980(2)$  Å. Traces of  $\text{NH}_3$

(20) (a) Herrmann, W. A.; Kuchler, J. G.; Felixberger, J. K.; Herdtweck, E.; Wagner, W. *Angew. Chem.* **1988**, *100*, 420–422; *Angew. Chem., Int. Ed. Engl.* **1988**, *27*, 394–396. (b) Kuchler, J. G. Ph.D. Thesis, Technische Universität München, 1990.

in the laboratory atmosphere were responsible for the slow but quantitative transformation of "poly-MTO" (1) to  $\text{NH}_4\text{ReO}_4$ .

(e) "Depolymerization" of MTO. Disk-shaped pressed samples of "poly-MTO" (ca. 150 bar) were measured after single crystals of MTO had grown out of the surface of such samples (approximately 2 weeks).<sup>1,3</sup> Reflections belonging to "poly-MTO",  $\text{ReO}_3$ , and MTO (orthorhombic space group  $Cmc2_1$  (no. 36);  $a = 7.586(1)$  Å,  $b = 10.426(1)$  Å,  $c = 5.106(1)$  Å) were recorded simultaneously.

(f) X-ray Structure Determination of  $(\text{CH}_3)_4\text{Re}_2\text{O}_4$ . This compound formed as yellow needles from aqueous "poly-MTO" suspensions (crystal data from ref 20 in brackets): crystal diameters  $0.05 \times 0.1 \times 0.4$  mm, monoclinic space group  $Pn$  (no. 7),  $a = 6.055(3)$  [6.086(1)] Å,  $b = 8.526(1)$  [8.564(1)] Å,  $c = 9.196(4)$  [9.234(2)] Å,  $\beta = 95.06(2)^\circ$  [95.08(2)°],  $V = 472$  [479]  $\times 10^6$  pm<sup>3</sup>;  $T = 23 \pm 1$  °C;  $Z = 2$ ,  $F(000) = 436$ ,  $Q_{\text{calcd}} = 3.520$  [3.440] g·cm<sup>-3</sup>, Enraf-Nonius CAD4,  $\lambda = 71.07$  pm (Mo K $\alpha$ , graphite monochromator). The diffraction data were recorded in the same way as described in ref 20. The structure of  $(\text{CH}_3)_4\text{Re}_2\text{O}_4$  was solved; it turned out to be isotopic with the previously published structure.<sup>20</sup>

(g) Neutron Diffraction Study of MTO. The presence of multiple twinning in single-crystals of  $\text{CH}_3\text{ReO}_3$  results in unsatisfactory structure refinements using single-crystal X-ray diffraction methods.<sup>21</sup> The structural model based on single-crystal results was improved using X-ray powder diffraction data and Rietveld analysis. The positions of the deuterium atoms were located by subsequent Rietveld refinements and difference Fourier analyses following neutron powder diffraction measurements (neutron powder diffractometer MANI/FRM-Garching). However, data were recorded at ambient temperature and sublimation of the MTO sample produced single crystals in the powder samples, resulting in strong preferred orientation effects. For this reason, a definitive low-temperature neutron powder structural study was performed using the high-resolution powder diffractometer (HRPD)<sup>22</sup> at the ISIS spallation source (Rutherford Appleton Laboratory, U.K.).

Time-of-flight neutron powder diffraction data were collected at 5 K using a standard "orange" helium flow cryostat on HRPD. A time-

(21) Kiprof, P.; Scherer, W. Unpublished results.

(22) Ibberson, R. M.; David, W. I. F.; Knight, K. S. Rutherford Appleton Laboratory: Report RAL-92-031; Oxon, Great Britain.

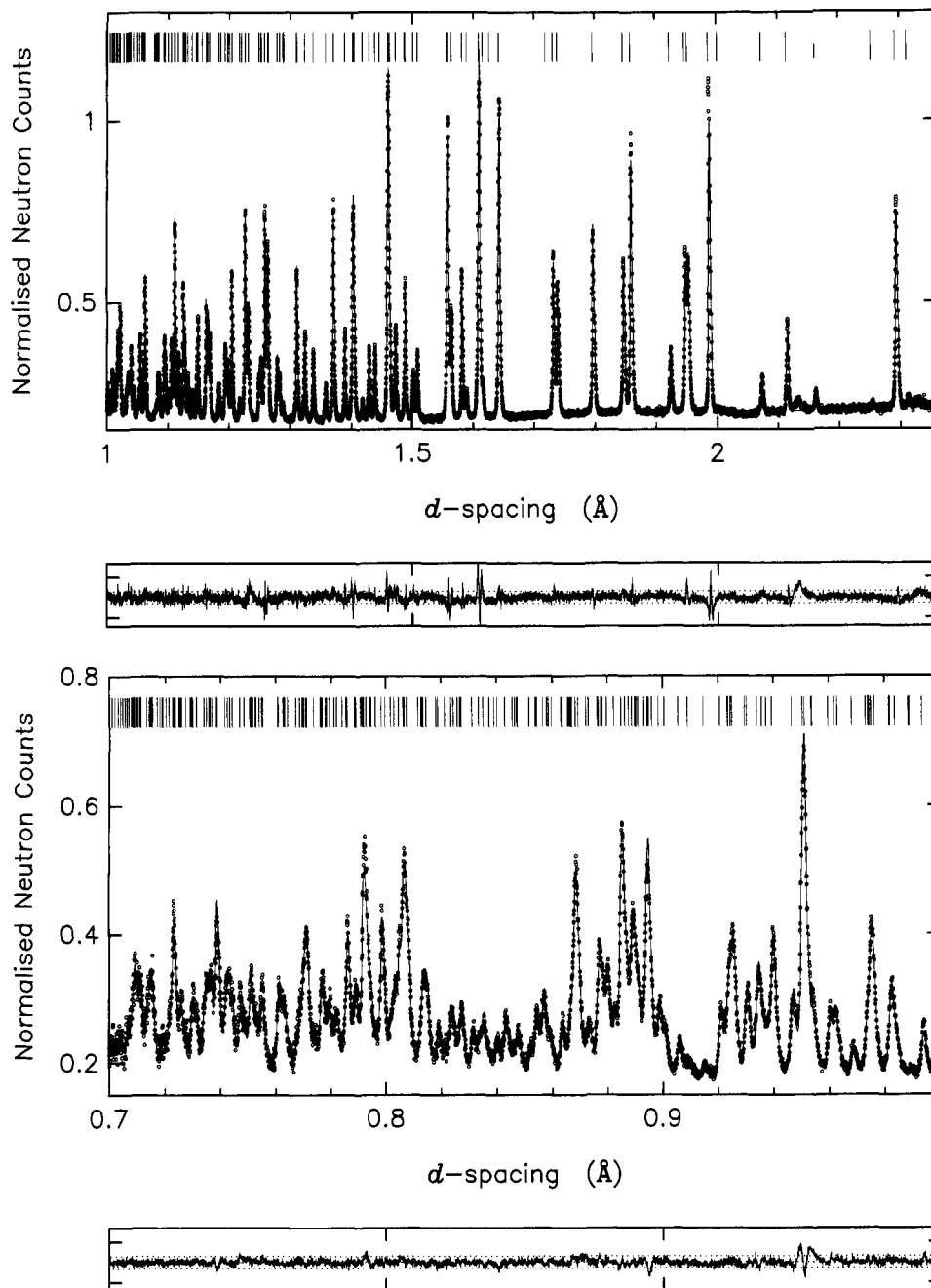


**Figure 16.** Observed (above) and calculated (below) diffraction profiles of MTO.

of-flight diffractometer such as HRPD utilizes a polychromatic neutron beam, and therefore, data are recorded by fixed angle detectors. Neutron wavelengths are discriminated by their time of arrival since  $t \propto 1/v_n \propto \lambda_n \propto d$ , where  $t$  is the time of flight,  $v_n$  is the neutron velocity,  $\lambda_n$  is the neutron wavelength, and  $d$  is the  $d$ -spacing of a particular Bragg reflection. For the present experiments at backscattering, with  $\langle 2\theta \rangle = 168^\circ$ , the time-of-flight range used was 30–130 ms, corresponding to a  $d$ -spacing range of between approximately 0.6 and 2.6 Å. Under these experimental settings, the diffraction data have an approximately constant resolution of  $\Delta d/d = 8 \times 10^{-4}$ . Data were recorded for a period of ca. 12 h, from a sample of mass ca. 8 g of fully deuterated MTO. Results of the final Rietveld analysis are as follows: orthorhombic space group  $Cmc2_1$  (no. 36),  $a = 7.383\ 41(1)$  Å,  $b = 10.310\ 29(2)$  Å,  $c = 5.008\ 43(1)$  Å,  $V = 381.267 \times 10^6$  pm<sup>3</sup>,  $T = 5 \pm 2$  K,  $Z = 4$ ,  $F(000) = 432$ ,  $\rho_{\text{calcd}} = 4.396$  g cm<sup>-3</sup>,  $R_p = \sum |Y_{\text{obsd}} - Y_{\text{calcd}}| / \sum Y_{\text{obsd}} = 3.11$ ,  $R_I = \sum |I_{\text{obsd}} - (1/C)I_{\text{calcd}}| / \sum I_{\text{obsd}} = 4.73$ ,  $R_{wp} = [\sum w |Y_{\text{obsd}} - Y_{\text{calcd}}|^2 / \sum w Y_{\text{obsd}}^2]^{1/2} = 3.74$ ,  $R_{\text{exptl}} = [(N - P + C) / \sum w Y_{\text{obsd}}^2]^{1/2} = 1.67$ ,  $\chi^2 = 1 / (N - P + C) \sum w |Y_{\text{obsd}} - Y_{\text{calcd}}|^2 = 5.01$  for 12 395 observations and 55 basic variables. The observed and calculated diffraction profiles are shown in Figure 16. A small amount of ReO<sub>3</sub> impurity is evident in the fit.

**Table 3.** Final Coordinates and Equivalent Thermal Displacement Parameters<sup>a</sup> of MTO

atom	$x/a$	$y/b$	$z/c$	$U(\text{eq})$ (Å <sup>2</sup> )
Re1	0	-0.172 19(6)	-0.250 00	$B = 0.08$ (2)
O1	-0.192 48(10)	-0.105 83(7)	-0.122 29(18)	0.0086 (5)
O2	0	-0.177 11(11)	-0.589 72(21)	0.0097 (7)
C1	0	-0.363 41(9)	-0.128 54(28)	0.0081 (6)
D1	0	-0.365 55(8)	0.087 36(32)	0.0237 (8)
D2	0.121 55(11)	-0.410 16(8)	-0.209 37(20)	0.0257 (6)

<sup>a</sup>  $U(\text{eq}) = 1/3$  of the trace of the orthogonalized  $U$ .

**(2) Electron Diffraction (ED) and TEM Studies.** Electron diffraction and TEM investigations were performed with a Philips EM 400 transmission electron microscope equipped with a high-magnification goniometer (HMG,  $\pm 25^\circ$  tilt). The microscope was operated at 100 kV (wavelength associated with electrons,  $\lambda = 0.037$  Å) and 120 kV ( $\lambda = 0.033\ 48$  Å), respectively. The camera length used was  $L = 180$  mm. A photographic enlargement  $V = 8.46$  was chosen for all prints of electron diffraction pattern images. Copper grids (400 mesh, diameter 3 mm) coated with perforated carbon foil were used to hold the powdered sample. The samples were mixed with water and carefully ground in an agate mortar. A drop of the resulting suspension

(23) Müller, U.; Klingelhöfer, P. *Z. Naturforsch.* **1983**, *38b*, 559–561.

**Table 4.** Anisotropic Thermal Displacement Parameters<sup>a</sup> of MTO

atom	<i>U</i> (11)	<i>U</i> (22)	<i>U</i> (33)	<i>U</i> (23)	<i>U</i> (13)	<i>U</i> (12)
O1	0.0025(4)	0.0160(5)	0.0073(2)	-0.0015	0.0021	0.0037
O2	0.0071(6)	0.0195(6)	0.0023(7)	-0.0006	0.0000	0.0000
C1	0.0084(6)	0.0089(6)	0.0071(6)	-0.0025	0.0000	0.0000
D1	0.0284(7)	0.0274(8)	0.0152(7)	0.0052	0.0000	0.0000
D2	0.0153(6)	0.0275(6)	0.0344(3)	-0.0025	0.0081	0.0053

<sup>a</sup> The temperature factor has the form of  $\exp(-T)$ , with  $T = 2\pi^2 \sum_i (h_i^2 U_{ij} a_i^* a_j^*)$  for anisotropic atoms.  $a_i^*$  are reciprocal axial lengths and  $h(i)$  are the reflection indices.

was placed onto a copper grid. Small crystal fragments or areas of about 2  $\mu\text{m}$  in diameter of crystalline flakes were investigated by selected area diffraction.

Electron diffraction patterns different from that of "poly-MTO" were discovered in only one sample (unpurified sample of **1**, prepared at room temperature). They were identified as a crystalline "impurity" with orthorhombic cell constants  $a = 18.00 \text{ \AA}$ ,  $b = 13.70 \text{ \AA}$ , and  $c = 18.10 \text{ \AA}$ . The cell constants of this impurity resemble those of  $\alpha\text{-NbBr}_5$ ,<sup>23</sup> which possesses a dimeric structure with two bridging bromo ligands. We suggest a similar dimeric structure consisting of oxo-bridged  $\{(\text{CH}_3)_3\text{ReO}_2\}_2$  units. (There is also a close structural relationship between  $(\text{CH}_3)_4\text{Re}_2\text{O}_4$  and the corresponding  $\text{NbCl}_4$  structure.)<sup>24</sup> The anionic trimeric fragment  $[(\text{CH}_3)_6\text{Re}_3\text{O}_6]^-$  is also known.<sup>25</sup> It is formed from the above  $(\text{CH}_3)_4\text{Re}_2\text{O}_4$  under reductive conditions and in the presence of small amounts of oxygen. The amounts of the as yet unknown impurity must be very small since it was not detectable by X-ray powder diffractometry or any other analytical method, e.g. IR and NMR spectroscopy. However, the impurity has not yet been detected in any other sample prepared at ordinary conditions ( $\Delta T \geq 70 \text{ }^\circ\text{C}$ ).

**(3) Wideline <sup>1</sup>H NMR Spectra.** The proton NMR spectra were obtained at 300.1 MHz on a Bruker MSL 300 spectrometer. A background-free <sup>1</sup>H selective probehead with a 5 mm solenoid coil was used. In order to avoid proton signals from a glass (Si-OH) or a Teflon (softeners) sample tube, a lump of the "poly-MTO" or of polycrystalline MTO, respectively, was placed directly into the coil. A proton 90° pulse length of 4  $\mu\text{s}$  was applied, and a dead-time delay of 10  $\mu\text{s}$  was sufficient to exclude ringing effects. The pulse repetition rate was 100 ms. Liquid H<sub>2</sub>O served as an external reference ( $\delta = 4.6 \text{ ppm}$ ). For further details see the caption of Figure 7.

**(4) TGA-MS Measurements** were performed with a thermobalance TGA 7 (Perkin Elmer) and a mass spectrometer QMG 420 (Balzers) coupled by means of a heated capillary. The samples were subjected to a temperature program with a 2 h segment at 70  $^\circ\text{C}$  for drying and a dynamic segment of heating at 10 K/min between 70 and 700  $^\circ\text{C}$ . The samples were held in an atmosphere of He (45 sccm, 1 bar).

The samples of compound **1** used in the TGA-MS measurements were freshly synthesized in D<sub>2</sub>O (99.3% isotopically enriched). In contrast to the described standard method,<sup>1</sup> compound **1** was washed only with D<sub>2</sub>O or H<sub>2</sub>O (see the following experimental descriptions) to remove HReO<sub>4</sub>.

**Experiment a:** Compound **1** synthesized and washed with D<sub>2</sub>O shows an initial weight loss of 85% (absorbed water) and is followed by a plateau (Figure 17). During a weight loss of 7.6% at 285  $^\circ\text{C}$ , one detects intercalated D<sub>2</sub>O, CH<sub>4</sub>, and CO<sub>2</sub> as well as H<sub>2</sub>O (from

(24) Taylor, D. R.; Calabrese, J. C.; Larsen, E. M. *Inorg. Chem.* **1977**, *16*, 721-722.

(25) Herrmann, W. A.; Albach, R. W.; Behm, J. *J. Chem. Soc., Chem. Commun.* **1991**, 367-369.

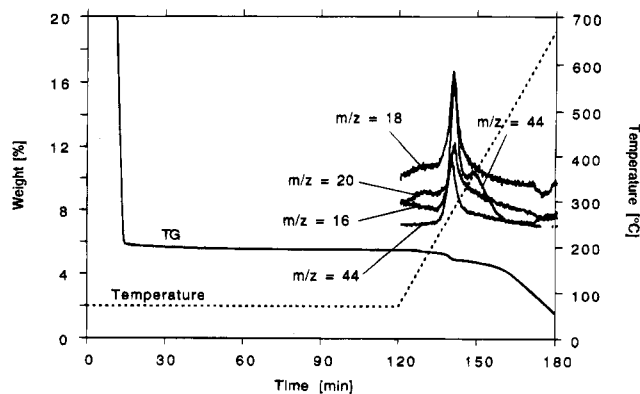


**Figure 17.** TG curve of a freshly prepared "poly-MTO" sample ( $\text{CH}_3\text{-ReO}_3$  in  $\text{D}_2\text{O}$ ). An initial weight loss of absorbed water (85%) is followed by a plateau. After heating to 285  $^\circ\text{C}$ , a weight loss of 7.6% of methane ( $m/z = 16$ ), intercalated D<sub>2</sub>O ( $m/z = 20$ ), carbon dioxide ( $m/z = 44$ ), and H<sub>2</sub>O ( $m/z = 18$ ) can be detected by MS.

combustion of methane:  $\text{CH}_4 + 4[\text{O}] \rightarrow \text{CO}_2 + 2\text{H}_2\text{O}$ ; [O] equivalents from the  $\text{ReO}_3$  fragment).

**Experiment b:** Compound **1** (synthesized with D<sub>2</sub>O and washed with H<sub>2</sub>O) showed similar results. A significant exchange of intercalated D<sub>2</sub>O against absorbed H<sub>2</sub>O is not observed. After heating to 277  $^\circ\text{C}$  a weight loss of 8.4% of intercalated D<sub>2</sub>O, CH<sub>4</sub>, CO<sub>2</sub>, and H<sub>2</sub>O (from combustion of methane, see above) can be detected by MS.

Nevertheless, it is difficult to quantify the amount of intercalated water because the observed weight loss of about 8% corresponds to D<sub>2</sub>O, CH<sub>4</sub>, CO<sub>2</sub> and H<sub>2</sub>O (the MS experiments cannot be used to quantify the individual amounts). Assuming a quantitative elimination of the methyl group as methane should result in a weight loss of about 6% (from stoichiometric considerations). Therefore the amount of intercalated water should be much smaller than 2% due to the additional weight loss by the combustion process:  $\text{CH}_4 + 4[\text{O}] \rightarrow \text{CO}_2 + 2\text{H}_2\text{O}$ ; [O] equivalents from the  $\text{ReO}_3$  fragment.

The exothermic reaction enthalpy of the elimination of methane was calorimetrically determined by a DSC 404 (Netzsch):  $\Delta H = -8 \text{ kJ/mol}$  (monomer).

**(5) FT-Raman Measurements** (J. Mink) were performed with a Bio-Rad Digilab dedicated Raman spectrometer using the 1064 nm Nd-YAG laser line for excitation. The laser power at the sample was between 30 and 100 mW.

**(6) Infrared Spectra** (J. Mink) were measured on a Bomem MB-102 Fourier-transform infrared spectrometer equipped with a CsI beam splitter and DTGS detector. Both transmission and emission techniques were used for the highly reflecting sample.

**Acknowledgment.** This work was supported by the Deutsche Forschungsgemeinschaft and the Fonds der chemischen Industrie. We thank Dr. E. Herdtweck of our institute for advice. We are also indebted to Prof. M. Jansen (Institut für Anorganische Chemie der Universität Bonn), Prof. U. Müller (Fachbereich Chemie der Universität Kassel), Prof. R. K. Harris (Department of Chemistry, University of Durham), and Prof. F. H. Köhler and Dr. R. A. Fischer of our institute for discussions. Prof. D. Babel (Fachbereich Chemie der Universität Marburg) is acknowledged for the pycnometrical measurements.